$S=1$ antiferromagnetic Heisenberg chain in a magnetic field

Tôru Sakai* and Minoru Takahashi
Institute for Solid State Physics, University of Tokyo, Roppongi, Minato-ku, Tokyo 106, Japan
(Received 15 November 1990; revised manuscript received 28 January 1991)

A one-dimensional $S=1$ Heisenberg antiferromagnet in a magnetic field $\mathbf{H}$ ($\|z$ axis) at $T=0$ is studied by numerical diagonalizations up to $N=16$. We give the magnetization curve at the thermodynamic limit, and derive an anomaly at H_{c1} ($=\Delta$), where Δ is the Haldane gap. It is also found that the transverse spin correlation has the asymptotic form $\langle S_0^x S_r^x \rangle \sim (-1)^r r^{-\eta}$, and the transverse staggered susceptibility $\chi_{\rm st}^{xx}$ diverges between H_{c1} and H_{c2} ($=4$). The exponent η has a minimum ($\eta \simeq 0.3$) at magnetization $m \simeq \frac{1}{3}$ and $\eta \simeq 0.5$ at H_{c1} and H_{c2}. If the system is quasi-one-dimensional, even small interchain couplings can create a canted Néel order, within a mean-field approximation for interchain interactions. This is consistent with a recent NMR measurement for $Ni(C_2H_8N_2)_2NO_2(ClO_4)$ (NENP) at low temperature.

I. INTRODUCTION

Haldane[1] predicted that a one-dimensional Heisenberg antiferromagnet has an energy gap for integral S, but not for half-integral S. This prediction has been supported by many theoretical studies, which are, for example, finite-size scaling,[2] numerical diagonalizations,[3,4] Monte Carlo calculations,[5] analyses of an exactly solvable model,[6] a variational method,[7] etc. The gap in the thermodynamic limit has been estimated to be $\Delta=0.411\pm0.001$ for $S=1$, using numerical diagonalization[4] up to $N=16$, which gives good agreement with the result of a Monte Carlo calculation,[5] 0.41. We use the unit such that the coupling constant of the exchange interaction is one.

On the other hand, some experimental studies[8–11] have also given the evidence of the Haldane gap for $Ni(C_2H_8N_2)_2NO_2(ClO_4)$, abbreviated NENP, which is an $S=1$ quasi-one-dimensional antiferromagnet. Although most real quasi-one-dimensional antiferromagnets have Néel order due to interchain interactions at low temperature, NENP has no Néel order at least down to 1.2 K. It was expected that, if the interchain interactions are small enough, the system has no Néel order even at $T=0$. This has been supported by some theoretical studies, which are a perturbative approach,[12] a field-theoretical analysis,[13] a mean-field approximation for interchain couplings,[14] and a rigorous proof in the reduced Hilbert space.[15] Using a mean-field approximation for interchain interactions, it has been shown[16] that NENP has no Néel order even at $T=0$. Thus the Haldane gap can exist also in a quasi-one-dimensional system such as NENP, which is intrinsically three dimensional.

High-field magnetization measurements[10,11] have also indicated the evidence of the Haldane gap for NENP. According to those experiments, a transition occurs from the nonmagnetic to magnetic state at H_{c1}, which supports the existence of an energy gap between the ground state with $\sum_j S_j^z=0$ and the first excited states with $\sum_j S_j^z=\pm1$. It is also noted that the curve of the field derivative dm/dH in an experiment[11] has an anomalous behavior at H_{c1}.

Recently, it has been reported that a NMR measurement[17] indicates a strong antiferromagnetic correlation for the magnetic state of NENP in such a high field as $H>H_{c1}$. Then it is expected that canted Néel order, that is, the state which has both ferromagnetic order along the z axis ($\|\mathbf{H}$) and antiferromagnetic sublattice order in the xy plane ($\perp\mathbf{H}$), exists at sufficiently low temperature.

In this paper we study a one-dimensional $S=1$ Heisenberg antiferromagnet in a magnetic field H at $T=0$ by numerical diagonalizations up to $N=16$. At first, we give the magnetization curve at the thermodynamic limit and derive an anomaly at H_{c1}. Next, we show that the transverse spin correlation $\langle S_0^x S_r^x \rangle$ decays algebraically and the transverse staggered susceptibility $\chi_{\rm st}^{xx}$ diverges in the whole region between H_{c1} and H_{c2}, where H_{c2} is the magnetic field which gives the saturated magnetization. Then we consider the quasi-one dimensional case and show that a transition from disorder to canted Néel order exists at H_{c1}, using a mean-field approximation for interchain interactions.

II. MAGNETIZATION CURVE

At first, we consider the magnetization process at $T=0$ for the ideal one-dimensional case. The Hamiltonian is

$$\mathcal{H}=\sum_j \mathbf{S}_j\cdot\mathbf{S}_{j+1}-H\sum_j S_j^z \ . \tag{1}$$

Actual Haldane magnets have the anisotropic term $D\sum_j S_j^{z2}+E\sum_j (S_j^{x2}-S_j^{y2})$. For simplicity we neglect this term. We define $E(N,M)$ as the lowest energy of the first term of (1) in the subspace where $\sum_j S_j^z=M$, for an N-site system. We calculate $E(N,M)$ ($M=0,1,2,\ldots,N$) under the periodic boundary condition for even-site systems up to $N=16$, using Lanczos' algorithm. The results are shown in Table I. Using those data, we give the magnetization curve at the thermodynamic limit. Correctly speaking, we do not give all the points of the curve, but

TABLE I. Numerical results of the lowest energy $E(N,M)$ of $\sum_j \mathbf{S}_j \cdot \mathbf{S}_{j+1}$ in the subspace where $M=\sum_j S_j^z$ for N-site systems.

M \ N	6	8	10	12	14	16
0	−8.6174	−11.3370	−14.0941	−16.8696	−19.6551	−22.4468
1	−7.8968	−10.7434	−13.5693	−16.3854	−19.1962	−22.0040
2	−6.4617	−9.5966	−12.2597	−15.5294	−18.4227	−21.2916
3	−4.3988	−7.8756	−11.1548	−14.2781	−17.3097	−20.2830
4	−1.4893	−5.6381	−9.2775	−12.6524	−15.8693	−18.9844
5	2	−2.9174	−6.9946	−10.6729	−14.1157	−17.4056
6	6	0.2984	−4.3257	−8.3592	−12.0641	−15.5578
7		4	−1.2672	−5.7244	−11.7284	−13.4527
8		8	2.1983	−2.7674	−9.1177	−11.1005
9			6	0.5232	−6.2319	−8.5076
10			10	4.1355	−3.0632	−5.6747
11				8	2.3902	−2.5965
12				12	6.0999	0.7321
13					10	4.3014
14					14	8.0767
15						12
16						16

give some points and connect them by a smooth curve as a guideline.

We define H_{c1} such that nonzero magnetization occurs for $H > H_{c1}$, and H_{c2} such that magnetization is saturated for $H > H_{c2}$. The Haldane gap, which is defined as Δ, is the energy gap between the ground state and triplet of the first excited states for the first term of (1). These first excited states are the lowest-energy states in the subspaces where $M=\pm 1$, respectively, and the second-lowest-energy state in the subspace where $M=0$.[1] Thus we get $\Delta=\lim_{N\to\infty}[E(N,1)-E(N,0)]$. At $H=E(N,1)-E(N,0)$, the ground state of the Hamiltonian (1) changes from nonmagnetic to magnetic for an N-site system. Therefore, $H_{c1}=\Delta$. In addition, since the ground state of (1) has saturated magnetization for $H>E(N,N)-E(N,N-1)$, we get $H_{c2}=\lim_{N\to\infty}[E(N,N)-E(N,N-1)]$. The lowest-energy state in the subspace where $M=N-1$ is exactly given by $N^{-1/2}\sum_{r=0}^{N-1}(-1)^r|\ldots 11011\ldots\rangle_r$, where $|\ldots 11011\ldots\rangle_r$ is the state with $S_r^z=0$ and $S_j^z=1$ $(j\neq r)$. The state has the energy $E(N,N-1)=N-4$, and $E(N,N)-E(N,N-1)=4$ is independent of N. Thus the critical field H_{c2} is given by $H_{c2}=4$. In this paper we do not write the g factor and Bohr magneton explicitly for simplicity.

It is well known that the conformal field theory[18] is a powerful method for one-dimensional quantum systems. It predicts that if the lowest-energy state is massless, the size-dependence of the energy per site has the form[19]

$$\lim_{N\to\infty}\frac{1}{N}E(N,M)=\varepsilon(m)+C(m)\frac{1}{N^2}\ , \tag{2}$$

where $m\equiv M/N$ is the magnetization and $\varepsilon(m)$ is the lowest energy per site at the thermodynamic limit. The second term represents the finite-size correction. It is noted that we must change N with $m=M/N$ fixed. Plots of $E(N,M)/N$ versus $1/N^2$ for $m=0$, $\frac{1}{4}$, $\frac{1}{2}$, and $\frac{3}{4}$ are shown in Fig. 1. The plot is almost linear for $m\neq 0$, but the value for $m=0$ converges faster than $1/N^2$. It suggests that the lowest-energy state is massless for $m\neq 0$, while massive only for $m=0$. Thus we assume that (2) is satisfied for $0<m<1$. In order to estimate $\varepsilon(m)$, we extrapolate from the largest- and next-largest-size values of $E(N,M)/N$ by the form (2). For example, we use $E(16,4)$ and $E(12,3)$ to determine $\varepsilon(\frac{1}{4})=-1.1823\pm 0.0002$. We estimate the error by the difference from the result extrapolated from the next- and next-next-largest-size data, which are $E(12,3)$ and $E(8,2)$ in the example. We can estimate $\varepsilon(m)$ by the extrapolation, for $m=\frac{1}{8}$, $\frac{1}{6}$, $\frac{1}{4}$, $\frac{1}{3}$, $\frac{5}{8}$, $\frac{1}{2}$, $\frac{3}{8}$, $\frac{2}{3}$, $\frac{3}{4}$, $\frac{5}{6}$, and $\frac{7}{8}$. The error due to extrapolation is smaller than 0.01% for $m=\frac{1}{4}$, $\frac{1}{2}$, and $\frac{3}{4}$. The error cannot be estimated for other values of m, because only two points can be used for extrapolation; for example, we can use only $N=8$ and 16 for $m=\frac{1}{8}$. But we think that these estimations are also sufficiently accurate to plot in the figure. In fact, the difference between the estimation of $\varepsilon(\frac{1}{2})$ extrapolated from $E(14,7)$ and $E(16,8)$, and the one extrapolated from $E(6,3)$ and $E(12,6)$, is about 0.03%. Thus we think that estimations even from only two points are as accurate as the latter estimation of $\varepsilon(\frac{1}{2})$, because the size dependence of $E(N,M)$ does not have a drastic change when m changes in the region $0<m<1$, where the universality class does not change. Estimated values of $\varepsilon(m)$ are plotted in Fig. 2, where the value of $\varepsilon(0)$ we use is from results of the Vanden Broech and Schwartz (VBS) method[20] as used by Betsuyaku.[21]

Minimizing the total energy of the system (1), $\varepsilon_{\text{tot}}=\varepsilon(m)-Hm$, it is found that the magnetization curve at $T=0$ is derived from

$$\varepsilon'(m)=H\ , \tag{3}$$

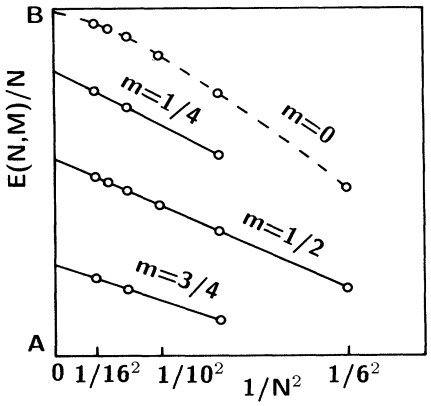

FIG. 1. Plots of $E(N,M)/N$ vs $1/N^2$ with $m=M/N=0$, $\frac{1}{4}$, $\frac{1}{2}$, and $\frac{3}{4}$ fixed, respectively. The origin is sifted along the vertical axis without changing the scale. The values of points A and B are as follows: A, -1.47, -1.24, -0.73, and -0.03; B, -1.40, -1.17, -0.66, and -0.10 for $m=0$, $\frac{1}{4}$, $\frac{1}{2}$, and $\frac{3}{4}$, respectively. The plots are almost linear for $m\neq 0$, which suggests that the lowest-energy states re massless.

at the thermodynamic limit. For a finite system it is derived from

$$m=\frac{M}{N}:M=\max[M|E(N,M)-E(N,M-1)<H]\ , \quad (4)$$

which gives an N-step curve. Now we assume that $\varepsilon(m)$ and $C(m)$ are analytic for $0<m<1$. In this region we use the form (2) to get the size dependence of the spin-excitation gap, which is

$$E(N,M+1)-E(N,M)\simeq\varepsilon'(m)+\tfrac{1}{2}\varepsilon''(m)\frac{1}{N}+O\left[\frac{1}{N^2}\right]. \quad (5)$$

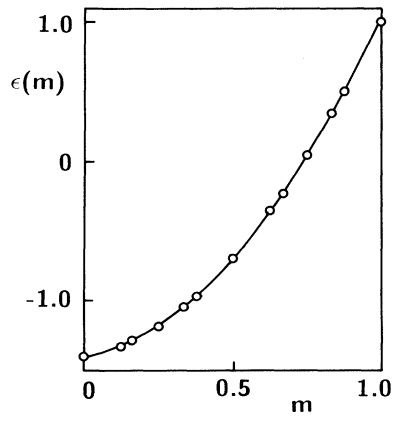

FIG. 2. Plot of the lowest energy per site $\varepsilon(m)$ vs m. Each point is derived from the largest- and next-largest-size data of $E(N,M)/N$ using the extrapolating form (2). The solid curve is only a guideline. As mentioned in the text, the error of each point is so small (we think it is within 0.1%) that we do not write it explicitly.

$$E(N,M)-E(N,M-1)\simeq\varepsilon'(m)-\tfrac{1}{2}\varepsilon''(m)\frac{1}{N}+O\left[\frac{1}{N^2}\right]. \quad (6)$$

In order to estimate $\varepsilon'(m)$, we plot $E(N,M+1)-E(N,M)$ and $E(N,M)-E(N,M-1)$ versus $1/N$ in Fig. 3. Those curves are almost linear, at least for $m=\frac{1}{4}$, $\frac{1}{2}$, and $\frac{3}{4}$. We use the largest- and next-largest-size data for $E(N,M+1)-E(N,M)$ to determine $\varepsilon'(m)$ by the first and second terms of (5), and do the same treatment using $E(N,M)-E(N,M-1)$ and the form (6). The two results of $\varepsilon'(m)$ coincide with each other with a difference of less that 1% of $m\geq 1/4$. Only for $\frac{1}{6}$ and $\frac{1}{8}$ is the difference a few percent. Thus we regard the average of the two results based on (5) and (6) as the extrapolated value of $\varepsilon(m)$ and the difference between the two as the error due to extrapolation. Now we consider the case of $m=0$. It is found that $E(N,1)-E(N,0)$ converges faster than $1/N$, as shown by points connected by the dashed curve in Fig. 3. Even if we extrapolate it linearly to $1/N$, the result would be finite (~ 0.32). This is also the evidence of the Haldane gap. Here we use the result of extrapolation by Shanks' transformation[22] in another paper[4] [$\Delta=\varepsilon'(0)\equiv\lim_{m\to 0+}\varepsilon'(m)=0.411\pm 0.001$]. This transformation will be introduced later [form (35)]. Using the extrapolated values of $\varepsilon'(m)$, we draw the magnetization curve at the thermodynamic limit based on (3) in Fig. 4. As mentioned above, the errors

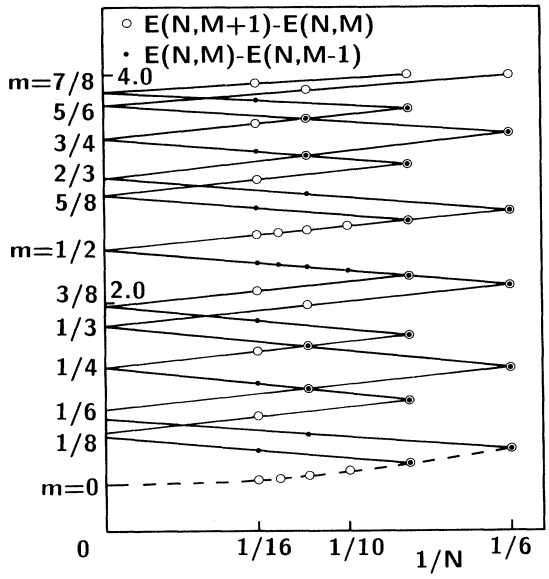

FIG. 3. Plots of spin-excitation gap vs $1/N$ with $m=M/N$ fixed. The plots are almost linear for $m=\frac{1}{4}$, $\frac{1}{2}$, and $\frac{3}{4}$. For $m\neq 0$, $E(N,M+1)-E(N,M)$ and $E(N,M)-E(N,M-1)$ coincide well at the thermodynamic limit ($N\to\infty$). For $m=0$, the gap $E(N,1)-E(N,0)$, which are connected by a dashed curve, converges faster than $1/N$ and has a finite value $\Delta=0.411\pm 0.001$ [this is the result of another paper (Ref. 4) by Shanks' transformation] at the thermodynamic limit.

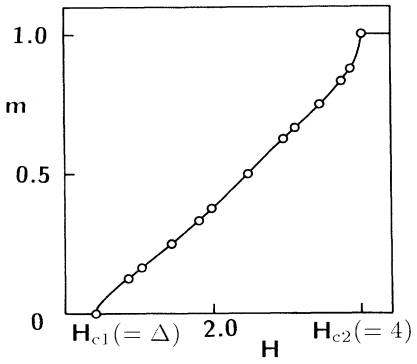

FIG. 4. Plot of m vs H $[=\varepsilon'(m)]$, that is, the magnetization curve at the thermodynamic limit. Each point is estimated by averaging the two results extrapolated by (5) and (6). For the extrapolation we use the largest- and next-largest size data of $E(N,M+1)-E(N,M)$ and $E(N,M)-E(N,M-1)$, respectively. We estimate the error of each point by the difference between the two results extrapolated by (5) and (6), but it is so small (less than a few percent) that we do not write it explicitly. The solid curve is a guideline. We use $H_{c1}=0.411$, which is the result of another paper (Ref. 4).

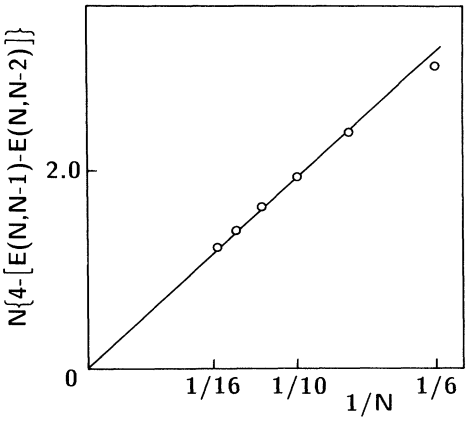

FIG. 5. Plot of $N\{4-[E(N,N-1)-E(N,N-2)]\}$ vs $1/N$. The extrapolated value is 0.01 ± 0.01. The result is estimated from the two points for $N=14$ and 16 by $1/N$ linear extrapolation, and the error is the difference from the result for $N=12$ and 14. It suggests $\varepsilon''(1)=0$.

are so small that we do not show them explicitly here. The solid line is a guideline to show nonlinear behaviors at H_{c1} and H_{c2}. The anomalous behavior at H_{c1} and H_{c2} will be discussed at the end of this section.

The field derivative dm/dH is derived from

$$\frac{dm}{dH}=\frac{1}{\varepsilon''(m)}\ , \tag{7}$$

at the thermodynamic limit. In order to estimate $\varepsilon''(m)$, we use the asymptotic form

$$N\{[E(N,M+1)-E(N,M)]-[E(N,M)-E(N,M-1)]\}$$
$$\simeq\varepsilon''(m)+(\tfrac{1}{2}\varepsilon^{(4)}(m)+C''(m))\frac{1}{N^2}+O\left[\frac{1}{N^4}\right]\ . \tag{8}$$

Extrapolating the quantity of the left-hand side of (8) by the same method as $\varepsilon(m)$ [fitting $\varepsilon''(m)+\text{const}/N^2$], we can estimate $\varepsilon''(m)$. We have checked that errors are less than a few percent by the same analysis as $\varepsilon(m)$. Now we want to know the value of $\varepsilon''(0)\equiv\lim_{m\to0+}\varepsilon''(m)$ and $\varepsilon''(1)\equiv\lim_{m\to1-}\varepsilon''(m)$. In order to estimate $\varepsilon''(1)$, we use the form

$$E(N,N-1)-E(N,N)-2)$$
$$\simeq\varepsilon'(1)-\frac{3}{2}\varepsilon''(1)\frac{1}{N}$$
$$+\left[\frac{7}{6}\varepsilon'''(1)+C'(1)\right]\frac{1}{N^2}+O\left[\frac{1}{N^3}\right]\ . \tag{9}$$

Since $\varepsilon'(1)\equiv\lim_{m\to1}\varepsilon'(m)=4$, we can estimate $\varepsilon''(1)$ by extrapolating $N\{4-[E(N,N-1)-E(N,N-2)]\}$ linearly to $1/N$, as shown in Fig. 5. The result is $\varepsilon''(1)=0.01\pm0.01$. Thus we conclude $\varepsilon''(1)=0$, that is, $dm/dH\to\infty$ at H_{c2}. The form of the anomaly at H_{c2} has been predicted as

$$m\sim1-\frac{2}{\pi}\left[1-\frac{H}{H_{c2}}\right]^{1/2}\ , \tag{10}$$

by a Bethe ansatz approach.[23] Assuming that the form is $m\sim1-A(1-H/H_{c2})^{\beta}$, and using the values of $\varepsilon''(\frac{5}{6})$ and $\varepsilon''(\frac{7}{8})$ estimated by our analysis, we get $A=0.66$ and $\beta=0.51$. Thus our result is almost consistent with (10).

At last we determine $\varepsilon''(0)$. Now we assume that $\varepsilon(m)$ is continuous at $m=0$ and the finite-size correction of $E(N,0)/N$ is less than $1/N^2$, that is

$$\frac{1}{N}E(N,0)\simeq\varepsilon(0)+o\left[\frac{1}{N^2}\right]\ , \tag{11}$$

where $\varepsilon(0)\equiv\lim_{m\to0+}\varepsilon(m)$. The absence of a correction larger than $1/N^2$ is supported by the plot of $E(N,0)/N$ versus $1/N^2$ in Fig. 1. Actually, it has been reported that the correction decays faster than $1/N^3$ by an analysis up to $N=14$. In addition, we assume

$$C(0)\equiv\lim_{m\to0+}C(m)=0\ . \tag{12}$$

The conformal field theory[19] brings the relation

$$C(m)=-\frac{\pi}{6}cv(m)\ , \tag{13}$$

where c is the central charge of the conformal anomaly (we have checked $c=1$ for $m\neq0$ numerically[24]), and $v(m)$ is the sound velocity, which is the derivative of the dispersion curve at the origin. Then the assumption (12) means $\lim_{m\to0+}v(m)=0$. This is valid if the dispersion curve near $k=\pi$ has $E\simeq[k-\pi)^2+\xi^{-2}]^{1/2}$ for $\sum_j S_j^z=1$.[25] Using (2), (11), and (12), we get

$$E(N,1)-E(N,0)\simeq\varepsilon'(0)+\varepsilon''(0)\frac{1}{N}+o\left[\frac{1}{N}\right]\ , \tag{14}$$

where $\varepsilon'(0)\equiv\lim_{m\to0+}\varepsilon'(m)$ and $\varepsilon''(0)\equiv\lim_{m\to0+}\varepsilon''(m)$.

On the other hand, the plot of $E(N,1)-E(N,0)$ versus $1/N$ in Fig. 3 suggests that the finite-size correction decays faster than $1/N$. Therefore, we conclude $\varepsilon''(0)=0$ and $dm/dH \to \infty$ at H_{c1}. If higher-order derivatives of $\varepsilon(m)$ at $m=0$ can be estimated, the form of divergence at H_{c1} can be determined. But it is difficult to estimate $\varepsilon'''(0)$ from $E(N,M)$ up to $N=16$, which is too small. This anomaly at H_{c1} has also been found in the curve of dm/dH based on a experiment[11] of NENP. We think that it could be seen clearer at a lower temperature. The existence of the anomaly at H_{c1} has been supported by the theory of three Majorana fermions,[26] the one of repulsive bosons,[27] and the field-theory method.[28] The curve of dm/dH based on the above analysis is shown in Fig. 6. Besides the two anomalies at H_{c1} and H_{c2}, there is a broad peak at $m \sim \frac{1}{2}$. We think that this peak is also a quantum effect.

III. TRANSVERSE SPIN CORRELATION

We consider the behavior of the transverse spin correlation $\langle S_0^x S_r^x \rangle$ in this section. We define $|M\rangle$ as the lowest-energy state of the first term of (1) in the subspace where $\sum_j S_j^z = M$. For $H < H_{c1}$ the ground state is $|0\rangle$, where the spin correlation is isotropic, and has the asymptotic form

$$\langle S_0^z S_r^z \rangle \sim (-1)^r r^{-1/2} \exp(-r/\xi) , \tag{15}$$

which was predicted by Haldane and has been supported by some numerical analyses.[29,30]

The analysis in the previous section suggests that the ground state is massless for $0<m<1$. Thus the transverse spin correlation is expected to have the asymptotic form

$$\langle S_0^x S_r^x \rangle \sim (-1)^r r^{-\eta} , \tag{16}$$

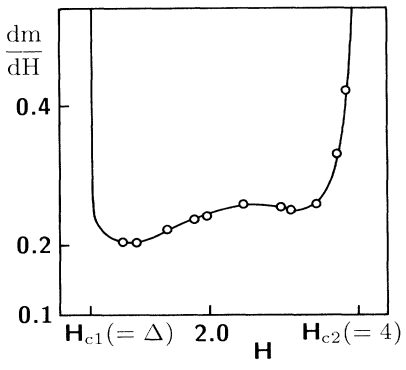

FIG. 6. Curve of the field derivative dm/dH $[=1/\varepsilon''(m)]$ at the thermodynamic limit derived from the extrapolation (8). We apply the same extrapolation as $\varepsilon(m)$ to estimate $\varepsilon''(m)$ here. The error is so small (less than a few percent) that we do not write it explicitly. In the test we show that dm/dH diverges at H_{c1} and H_{c2} because $\varepsilon''(0)=\varepsilon''(1)=0$ and has the form (10) near H_{c2}, but the analytic form near H_{c1} cannot be determined. The solid curve is a guideline to show the existence of these anomalies. A broad peak exists at $m \simeq \frac{1}{2}$.

for $H_{c1}<H<H_{c2}$ at $T=0$. We calculate $\langle S_0^x S_r^x \rangle$ up to $N=16$ numerically, as shown in Table II, and show plots of $\ln[(-1)^r \langle S_0^x S_r^x \rangle]$ versus $\ln r$ for $N=16$ in Fig. 7, where the dashed line is the plot for $M=0$ and the solid lines are for $M \neq 0$. It is found that the transverse spin correlation for $M=0$ decays faster than the others. In order to check the form (16) more clearly, we consider the size dependence of the transverse structure factor at wave vector $k=\pi$, defined by

$$S_\pi^x(N) = \sum_{r=0}^{N-1} (-1)^r \langle S_0^x S_r^x \rangle . \tag{17}$$

When the transverse spin correlation has the form (16), $S_\pi^x(N)$ depends on the system size as

$$S_\pi^x(N) \sim N^{1-\eta} , \tag{18}$$

for sufficiently large N. In Fig. 8 we plot $\ln S_\pi^x(N)$ versus $\ln N$ for $m=0$, $\frac{1}{4}$, $\frac{1}{2}$, and $\frac{3}{4}$, up to $N=16$. It is found that the plots are almost linear for $m=\frac{1}{4}$, $\frac{1}{2}$, and $\frac{3}{4}$, which suggests that the transverse spin correlation has the form (16) for $0<m<1$. Assuming the form (18), we estimate the value of η by

$$\eta = 1 - \ln\left[\frac{S_\pi^x(N)}{S_\pi^x(N')}\right] \Big/ \ln\left[\frac{N}{N'}\right] , \tag{19}$$

for $N \neq N'$. The values of η calculated by (19) with $N'=N+2$ for $m=\frac{1}{2}$, $N'=N+4$ for $m=\frac{1}{4}$, and $\frac{3}{4}$, are shown in Table III. Since those values converge well, we estimate η as the value derived from the largest pair (N,N') we can use, even for other values of m. Our estimations of η are shown in Table IV. We determine the error of η by the difference between the values derived from the largest pair (N,N') and the one derived from the next-largest pair (N,N'). We plot η versus m in Fig. 9, where we can use only one pair (N,N') to estimate η by (19) for $m=\frac{1}{8}$, $\frac{1}{6}$, $\frac{1}{3}$, $\frac{3}{8}$, $\frac{5}{8}$, $\frac{2}{3}$, $\frac{5}{6}$, and $\frac{7}{8}$. The accuracy of

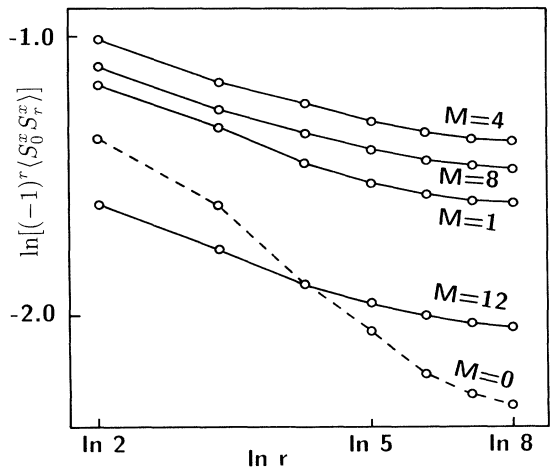

FIG. 7. Plots of $\ln(-1)^r \langle S_0^x S_r^x \rangle$ vs $\ln r$ for $N=16$. It is found that the transverse spin correlation decays faster for $M=0$ (dashed curve) than $M \neq 0$ (solid curves).

TABLE II. Numerical results of the transverse correlation function $\langle S_0^x S_r^x \rangle$ for the lowest-energy state of $\sum_j \mathbf{S}_j \cdot \mathbf{S}_{j+1}$ in the subspace $M = \sum_j S_j^z$, for N-site systems.

M \ r	0	1	2	3	4	5	6	7	8
				(i) $N=6$					
0	0.6667	−0.4787	0.2884	−0.2861					
1	0.7111	−0.5182	0.3854	−0.3622					
2	0.7123	−0.4853	0.3915	−0.3580					
3	0.6984	−0.4133	0.3544	−0.3306					
4	0.6575	−0.3048	0.2669	−0.2485					
5	0.5833	−0.1667	0.1667	−0.1667					
6	0.5	0	0	0					
				(ii) $N=8$					
0	0.6667	−0.4724	0.2721	−0.2409	0.2156				
1	0.7024	−0.5108	0.3558	−0.3223	0.3147				
2	0.7106	−0.4999	0.3758	−0.3342	0.3310				
3	0.7096	−0.4653	0.3732	−0.3310	0.3239				
4	0.6971	−0.4084	0.3413	−0.3047	0.2964				
5	0.6694	−0.3309	0.2817	−0.2507	0.2429				
6	0.6223	−0.2360	0.2100	−0.1853	0.1755				
7	0.5625	−0.125	0.125	−0.125	0.125				
8	0.5	0	0	0	0				
				(iii) $N=10$					
0	0.6667	−0.4698	0.2639	−0.2214	0.1848	−0.1818			
1	0.6966	−0.5048	0.3378	−0.3005	0.2813	−0.2742			
2	0.7071	−0.5038	0.3630	−0.3197	0.3042	−0.2946			
3	0.7112	−0.4861	0.3720	−0.3243	0.3092	−0.3028			
4	0.7077	−0.4531	0.3630	−0.3164	0.3005	−0.2955			
5	0.6964	−0.4061	0.3355	−0.2939	0.2778	−0.2732			
6	0.6757	−0.3459	0.2904	−0.2538	0.2389	−0.2347			
7	0.6428	−0.2742	0.2348	−0.2027	0.1886	−0.1857			
8	0.5989	−0.1923	0.1756	−0.1562	0.1414	−0.1358			
9	0.55	−0.1	0.1	−0.1	0.1	−0.1			
10	0.5	0	0	0	0	0			
				(iv) $N=12$					
0	0.6667	−0.4686	0.2592	−0.2108	0.1681	−0.1540	0.1454		
1	0.6924	−0.5001	0.3254	−0.2857	0.2604	−0.2487	0.2466		
2	0.7037	−0.5041	0.3526	−0.3090	0.2877	−0.2733	0.2718		
3	0.7098	−0.4955	0.3664	−0.3176	0.2984	−0.2852	0.2822		
4	0.7104	−0.4753	0.3676	−0.3171	0.2980	−0.2862	0.2825		
5	0.7060	−0.4449	0.3565	−0.3081	0.2883	−0.2776	0.2741		
6	0.6960	−0.4049	0.3324	−0.2883	0.2687	−0.2587	0.2555		
7	0.6795	−0.3557	0.2962	−0.2565	0.2380	−0.2288	0.2258		
8	0.6548	−0.2983	0.2515	−0.2158	0.1985	−0.1904	0.1874		
9	0.6216	−0.2337	0.2039	−0.1748	0.1572	−0.1505	0.1493		
10	0.5828	−0.1620	0.1510	−0.1370	0.1237	0.1144	0.1110		
11	0.5417	−0.0833	0.0833	−0.0833	0.0833	−0.0833	0.0833		
12	0.5	0	0	0	0	0	0	0	0
				(v) $N=14$					
0	0.6667	−0.4680	0.2562	−0.2044	0.1581	−0.1382	0.1236	−0.1212	
1	0.6892	−0.4963	0.3162	−0.2746	0.2454	−0.2314	0.2249	−0.2218	
2	0.7006	−0.5031	0.3440	−0.3004	0.2757	−0.2590	0.2526	−0.2485	
3	0.7076	−0.4997	0.3601	−0.3117	0.2895	−0.2727	0.2659	−0.2632	
4	0.7104	−0.4872	0.3664	−0.3149	0.2937	−0.2781	0.2705	−0.2683	
5	0.7095	−0.4668	0.3637	−0.3121	0.2905	−0.2762	0.2686	−0.2663	

TABLE II. (*Continued*).

r / M	0	1	2	3	4	5	6	7	8
6	0.7047	−0.4390	0.3519	−0.3027	0.2807	−0.2673	0.2600	−0.2577	
7	0.6958	−0.4041	0.3306	−0.2851	0.2635	−0.2508	0.2439	−0.2417	
8	0.6821	−0.3626	0.3004	−0.2587	0.2382	−0.2263	0.2197	−0.2178	
9	0.6625	−0.3149	0.2633	−0.2252	0.2059	−0.1950	0.1889	−0.1871	
10	0.6366	−0.2617	0.2232	−0.1895	0.1706	−0.1615	0.1561	−0.1539	
11	0.6054	−0.2034	0.1811	−0.1567	0.1385	−0.1287	0.1254	−0.1248	
12	0.5712	−0.1398	0.1323	−0.1221	0.1115	−0.1024	0.0962	−0.0941	
13	0.5357	−0.0714	0.0714	−0.0714	0.0714	−0.0714	0.0714	−0.0714	
14	0.5	0	0	0	0	0	0	0	
				(vi) $N=16$					
0	0.6667	−0.4676	0.2543	−0.2003	0.1517	−0.1285	0.1102	−0.1023	0.0984
1	0.6867	−0.4933	0.3089	−0.2659	0.2339	−0.2183	0.2092	−0.2038	0.2030
2	0.6979	−0.5017	0.3367	−0.2931	0.2661	−0.2484	0.2393	−0.2324	0.2315
3	0.7053	−0.5014	0.3539	−0.3063	0.2820	−0.2633	0.2542	−0.2482	0.2467
4	0.7093	−0.4939	0.3630	−0.3119	0.2889	0.2709	0.2614	−0.2558	0.2539
5	0.7104	−0.4799	0.3651	−0.3124	0.2897	−0.2729	0.2630	−0.2576	0.2558
6	0.7085	−0.4600	0.3604	−0.3083	0.2852	−0.2695	0.2596	−0.2544	0.2527
7	0.7037	−0.4345	0.3485	−0.2988	0.2756	−0.2606	0.2511	−0.2460	0.2756
8	0.6957	−0.4037	0.3294	−0.2830	0.2603	−0.2459	0.2369	−0.2320	0.2304
9	0.6839	−0.3677	0.3035	−0.2605	0.2387	−0.2252	0.2166	−0.2120	0.2105
10	0.6678	−0.3270	0.2721	−0.2323	0.2116	−0.1990	0.1910	−0.1867	0.1852
11	0.6469	−0.2819	0.2376	−0.2012	0.1813	−0.1702	0.1627	−0.1586	0.1575
12	0.6214	−0.2328	0.2018	−0.1713	0.1516	−0.1414	0.1357	−0.1318	0.1301
13	0.5927	−0.1799	0.1632	−0.1433	0.1263	−0.1150	0.1094	−0.1076	0.1073
14	0.5623	−0.1229	0.1176	−0.1101	0.1018	−0.0938	0.0874	−0.0831	0.0817
15	0.5313	−0.0625	0.0625	−0.0625	0.0625	−0.0625	0.0625	−0.0625	0.0625
16	0.5	0	0	0	0	0	0	a	0

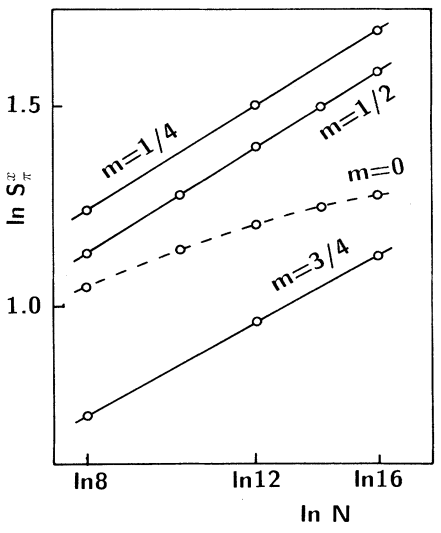

FIG. 8. Plots of $\ln S^x_\pi$ vs $\ln N$ with $m=0$, $\frac{1}{4}$, $\frac{1}{2}$, and $\frac{3}{4}$ fixed, respectively. The plots are almost linear for $m\neq 0$ (solid curves), while not for $m=0$ (dashed curve).

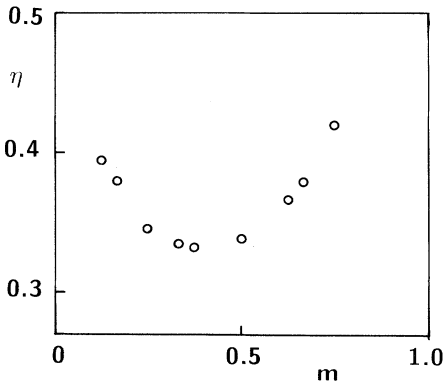

FIG. 9. Curve of the exponent η estimated by (19). We use only the largest pair (N,N') up to $N=16$ for each m. For example, $(N,N')=(14,16)$ for $m=\frac{1}{2}$, (6,12) for $m=\frac{1}{3}$. The error is estimated from the next-largest pair (N,N'), but it is so small (less than a few percent) that we do not write it explicitly. It is found that η has a minimum at $\eta\simeq\frac{1}{3}$ and η is about 0.5 at $m=0$ and 1.

TABLE III. Transverse structure factor at $k=\pi$ and exponent η estimated by (19) up to $N=16$ for $m=\frac{1}{4}, \frac{1}{2}$, and $\frac{3}{4}$. η converges well.

	$m=\frac{1}{4}$		$m=\frac{1}{2}$		$m=\frac{3}{4}$	
N	S^x_π	η	S^x_π	η	S^x_π	η
6			2.5644			
				0.3381		
8	3.4613		3.1023		2.0606	
				0.3378		
10		0.3428	3.5963			0.4161
				0.3379		
12	4.5181		4.0578		2.6110	
				0.3382		
14		0.3451	4.4936			0.4207
				0.3386		
16	5.4549		4.9085		3.0845	

these estimations cannot be determined, but based on the size dependence of η for $m=\frac{1}{4}, \frac{1}{2}$, and $\frac{3}{4}$, in Table III, we think that the errors are also within a few percent for other values of m because the size dependence does not have a drastic change as mentioned in the previous section. Thus we do not show the errors explicitly in Fig. 9. It is noted that the curve of η has a minimum at $m\simeq\frac{1}{3}$, which means that the transverse spin correlation is the strongest there. Such a minimum exists for $S\geq 1$, although the curve is monotonous for $S=\frac{1}{2}$.[31] We have checked it at least for $S=1$, $\frac{3}{2}$, and 2. It is also found that $\eta\simeq 0.5$ at H_{c1} and H_{c2} in Fig. 9. Since we do not know the analytic behavior of η for $m\sim 0$ and 1, we fit the quadratic function to three points nearest to $m=0$ and 1, respectively, in Fig. 9, to estimate η at H_{c1} and H_{c2}, respectively. Thus these are rough estimations, and we write only one digit here. It is consistent with Schulz's statement.[32] He conjectured that $\eta=\frac{1}{2}$ at H_{c1}, by representing a spin-1 operator as the sum of two spin-$\frac{1}{2}$ operators.

IV. QUASI-ONE-DIMENSIONAL CASE

We consider the quasi-one-dimensional case in this section. The system is represented by the Hamiltonian (1) with interchain interactions defined by

$$\mathcal{H}'=J\sum_{\langle ij\rangle}{}' \mathbf{S}_i\cdot\mathbf{S}_j \ , \tag{20}$$

where $\sum'$ is the sum about all the nearest-neighbor pairs that connect adjacent chains. Here we treat interchain interactions by a mean-field approximation,[14,16] which is effective for $J\ll 1$. Now we define the critical value J_c such that the ground state has Néel order for $J>J_c$, while not for $J_c>J>0$. The mean-field approximation for interchain interactions yields

$$J_c=\frac{1}{Z\chi^{\alpha\alpha}_{\rm st}} \ , \tag{21}$$

where $\chi^{\alpha\alpha}_{\rm st}$ is the staggered susceptibility of one-dimensional system described by the Hamiltonian (1), α is the easy axis of staggered magnetization ($\alpha=x$ or y for $H>0$), and Z is the number of adjacent chains [$Z=2$ or 4 for NENP (Ref. 16)]. Thus, within this approximation, we have only to calculate the transverse staggered susceptibility for the one-dimensional system at $T=0$, which is defined by

$$\chi^{xx}_{\rm st}=\frac{2}{N}\sum_l \frac{|\langle l|\hat{M}^x_{\rm st}|g\rangle|^2}{\mathcal{E}_l-\mathcal{E}_g} \ , \tag{22}$$

where

$$\hat{M}^x_{\rm st}=\sum_j (-1)^j S^x_j \ , \tag{23}$$

$|g\rangle$ is the ground state, $|l\rangle$ is the excited state, and $\mathcal{E}_g, \mathcal{E}_l$ are their energies, respectively, for the Hamiltonian (1) at finite H. We calculate $\chi^{xx}_{\rm st}$ at $T=0$ numerically as follows: At first, using the Lanczos algorithm, we get the wave function of the ground state for the Hamiltonian (1) with a staggered magnetic field described by

$$\mathcal{H}''=-h\sum_j (-1)^j S^x_j \ . \tag{24}$$

Next, we calculate the transverse staggered magnetizaton $\langle M^x_{\rm st}\rangle$ for this state. At last, we differentiate it with respect to h numerically to estimate $\chi^{xx}_{\rm st}$. Thus our numerical calculation is based on

$$\chi^{xx}_{\rm st}=\frac{1}{N}\frac{\partial\langle\hat{M}^x_{\rm st}\rangle}{\partial h}\bigg|_{h=0} \ , \tag{25}$$

rather than (22). We use this method to calculate $\chi^{xx}_{\rm st}$ up to $N=12$. This method can be used to calculate $\chi^{xx}_{\rm st}$ at most up to $N=14$, because $\sum_j S^x_j$ is not conserved, owing to the staggered magnetic field (24), and the dimension of

TABLE IV. Exponents η and ω estimated by (19) and (31), respectively, for $m=\frac{1}{4}, \frac{1}{2}$, and $\frac{3}{4}$. The scaling relation $\omega=2-\eta$ is satisfied within the errors.

m	$m=1/4$	$m=1/2$	$m=3/4$
η	0.345±0.003	0.339±0.001	0.421±0.005
ω	1.66 ±0.04	1.65 ±0.01	1.55 ±0.01

the Hilbert space used for calculation becomes larger. However, the direct calculation based on (22) is available only for smaller systems. The behavior of $\chi_{\rm st}^{xx}$ for $N=12$ is shown as a dashed curve in Fig. 10. It is found that $\chi_{\rm st}^{xx}$ diverges at each level-crossing point, which is defined by $H_M \equiv E(N,M)-E(N,M-1)$ $(\lim_{N\to\infty} H_1 = H_{c1}, \quad H_N = H_{c2})$. The form of the divergence at each H_M is

$$\chi_{\rm st}^{xx} \simeq \frac{1}{|H-H_M|} \ . \tag{26}$$

In particular, for $H > H_{c2}$, $\chi_{\rm st}^{xx}$ can be calculated analytically because the ground state is completely ferromagnetic here, and we get

$$\chi_{\rm st}^{xx} = \frac{1}{H-H_{c2}} \quad (H > H_{c2}) \ , \tag{27}$$

which is independent of N. Now we define the quantity

$$\tilde{\chi}_{\rm st}^{xx} \equiv \frac{2}{N} \frac{|\langle M|\hat{M}_{\rm st}^{x}|M-1\rangle|^2}{H-H_M} + \frac{2}{N} \frac{|\langle M+1|\hat{M}_{\rm st}^{x}|M\rangle|^2}{H_{M+1}-H} \ , \tag{28}$$

for $H_M < H < H_{M+1}$ $(1 \le M \le N-1)$. This satisfies the inequality

$$\chi_{\rm st}^{xx} \ge \tilde{\chi}_{\rm st}^{xx} \ . \tag{29}$$

$\tilde{\chi}_{\rm st}^{xx}$ gives a good approximation of $\chi_{\rm st}^{xx}$. According to our check, $\chi_{\rm st}^{xx}$ and $\tilde{\chi}_{\rm st}^{xx}$ coincide within 0.4% and the difference between them decreases as H approaches H_M, at least up to $N=14$. Since the system (1) is massless between H_{c1} and H_{c2} as shown in Sec. II, we think that $\chi_{\rm st}^{xx}$ always diverges in this region, as shown by the solid curve in Fig. 10. In order to make sure of it, we check that the numerator $(2/N)|\langle M+1|\hat{M}_{\rm st}^{x}|M\rangle|^2$ diverges as

$$\lim_{N\to\infty} \frac{2}{N} |\langle M+1|\hat{M}_{\rm st}^{x}|M\rangle|^2 = N^{\sigma} \ , \tag{30}$$

with $m=M/N$ fixed. Plots of $\ln[(2/N)|\langle M+1|\hat{M}_{\rm st}^{x}|M\rangle|^2]$ versus $\ln N$ for $m=0$, $\frac{1}{4}$, $\frac{1}{2}$, and $\frac{3}{4}$ are shown in Fig. 11. They look linear for $m\neq 0$, which suggests that (30) is valid and $\chi_{\rm st}^{xx}$ diverges for $H_{c1} < H < H_{c2}$. In order to consider the size dependence of $\chi_{\rm st}^{xx}$, we define $\tilde{\chi}_{\rm st}^{xx}$ as the value of $\tilde{\chi}_{\rm st}^{xx}$ at $H=(H_M+H_{M+1})/2$ and take $\bar{\chi}_{\rm st}^{xx}$ as an approximation of $\chi_{\rm st}^{xx}$ for $m=M/N$. We have checked the form

$$\lim_{N\to\infty} \bar{\chi}_{\rm st}^{xx} = N^{\omega} \ , \tag{31}$$

with fixed $m=M/N=\frac{1}{4}$, $\frac{1}{2}$, and $\frac{3}{4}$, respectively, up to $N=16$. The values of ω, which are estimated by applying (31) to $\bar{\chi}_{\rm st}^{xx}$, are shown in Table IV. It is found that the scaling relation

$$\omega = 2-\eta \tag{32}$$

is satisfied within the errors for $m=\frac{1}{4}$, $\frac{1}{2}$, and $\frac{3}{4}$. The relation (32) is of two-dimensional classical systems and is also derived from the conformal invariance.[18] Therefore, this analysis is consistent with the result in Sec. III.

Now we determine the asymptotic form of $\chi_{\rm st}^{xx}$ for $H \sim H_{c1}$ $(H < H_{c1})$. Here we also define $\bar{\chi}_{\rm st}^{xx}$ as

$$\tilde{\chi}_{\rm st}^{xx} \equiv \frac{2}{N} |\langle 1|\hat{M}_{\rm st}^{x}|0\rangle|^2 \left[\frac{1}{H_{c1}-H} + \frac{1}{H_{c1}+H} \right] , \tag{33}$$

where we use $\langle -1|\hat{M}_{\rm st}^{x}|0\rangle = \langle 1|\hat{M}_{\rm st}^{x}|0\rangle$. According to our numerical checkup to $N=14$, $\tilde{\chi}_{\rm st}^{xx}$ is also a good approximation for $0 \le H < H_{c1}$, and the difference between $\tilde{\chi}_{\rm st}^{xx}$ and $\chi_{\rm st}^{xx}$ decreases as H approaches H_{c1}. It suggests that only the first term of (33) contributes to the divergence of $\chi_{\rm st}^{xx}$ at H_{c1}. In order to make sure of it, we consider the second lowest-energy state which has a nonzero matrix element of $\hat{M}_{\rm st}^{x}$ with $|0\rangle$. This state must be in the subspace where $\sum_j S_j^z = 1$ and $k=\pi$. We define $|1\rangle_2$ as the second-lowest-energy state in the subspace and $E_2(N,1)$ as its energy for an N-site system. We calculate

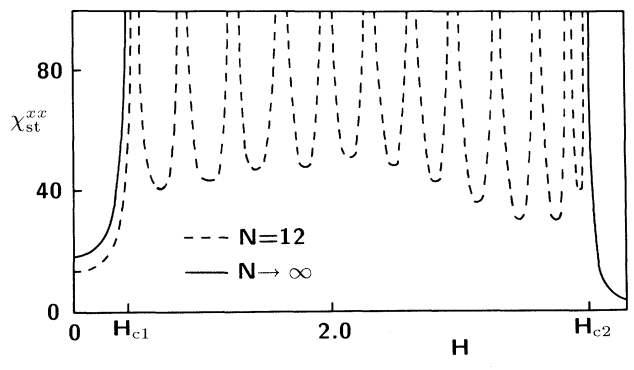

FIG. 10. Transverse staggered susceptibility $\chi_{\rm st}^{xx}$ at $T=0$ plotted vs H for $N=12$ (dashed curve) and the thermodynamic limit (solid curve). The latter always diverges between H_{c1} and H_{c2}, and has the asymptotic form $\chi_{\rm st}^{xx} \simeq (H_{c1}-H)^{-1}$ at $H \simeq H_{c1}(H < H_{c1})$. The form $\chi_{\rm st}^{xx} = (H-H_{c2})^{-1}$ for $H > H_{c2}$ is independent of N.

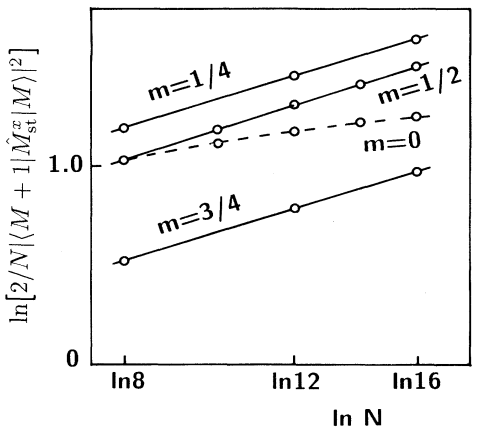

FIG. 11. Plots of $\ln(2/N)|\langle M+1|\hat{M}_{\rm st}^{x}|M\rangle|^2]$ vs $\ln N$ with $m=0$, $\frac{1}{4}$, $\frac{1}{2}$ and $\frac{3}{4}$ fixed, respectively. The plots are almost linear for $m\neq 0$ (solid curves), which suggest that the numerator of (28) diverges as $(2/N)|\langle M+1|\hat{M}_{\rm st}^{x}|M\rangle|^2 \sim N^{\sigma}$.

$E_2(N,1)$ up to $N=16$ and plot $E_2(N,1)-E(N,1)$ versus $1/N$ in Fig. 12. It suggests that there is a gap between $|1\rangle_2$ and $|1\rangle$ even at the thermodynamic limit. The estimated value of this gap is $E_2(N,1)-E(N,1) \to 0.563\pm0.001$ $(N\to\infty)$. Therefore, we conclude that the asymptotic behavior of $\chi^{xx}_{\rm st}$ for $H\sim H_{c1}$ $(H<H_{c1})$ is determined only by the first term of (33), because no other term of (22) diverges at H_{c1}. Since $\chi^{xx}_{\rm st}$ is finite at $H=0$, the factor $(2/N)|\langle 1|\hat{M}^x_{\rm st}|0\rangle|^2$ is finite at the thermodynamic limit. Thus we use Shanks' transformation[4,22] to estmate the value of $(2/N)|\langle 1|\hat{M}^x_{\rm st}|0\rangle|^2$ at the thermodynamic limit. The transformation is one of techniques for accelerating the convergence of a sequence $\{P_n\}$ to its limit P_∞, when $\{P_n\}$ satisfies

$$P_n = P_\infty + O(e^{-cn}), \quad n\to\infty , \tag{34}$$

where c is a constant.[33] The asymptotic form (34) is characteristic of data from a finite lattice when the system is not critical even at the thermodynamic limit. The algorithm of applying this transformation to a sequence $\{P_n\}$ is given by

$$P'_n = \frac{P_{n-1}P_{n+1}-P_n^2}{P_{n-1}+P_{n+1}-2P_n} . \tag{35}$$

If $\{P_n\}$ is exactly of the form (34), then P'_n is exactly P_∞; otherwise, P'_n approaches P_∞ more rapidly than P_n. Since three data (P_{n-1}, P_n, and P_{n+1}) are needed to determine P'_n by (35), the number of data of P'_n is less than P_n by 2. If sufficient data are available to apply (35) to P'_n again and determine P''_n, P''_n approaches P_∞ more rapidly than P'_n. Then we can get the best value for P_∞ by applying the transformation as many times as we can. In addition, it was shown[34] that the transformation can be used to estimate the limit P_∞, when $\{P_n\}$ satisfies the condition

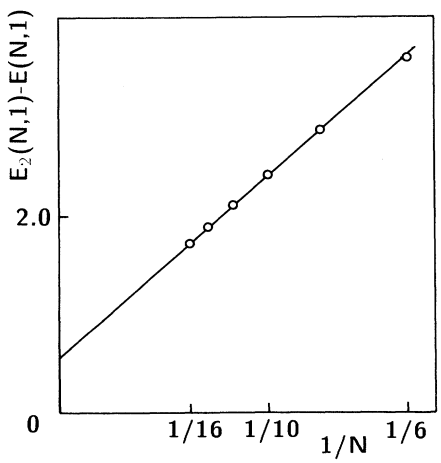

FIG. 12. Plot of $E_2(N,1)-E(N,1)$ vs $1/N$. It suggests that a finite gap exists between the lowest- and second-lowest-energy states in the subspace where $\sum_j S^z_j=1$ and $k=\pi$, even at the thermodynamic limit. The estimated gap is 0.563 ± 0.001. Here we use the same extrapolation as in Fig. 5.

TABLE V. Results of the Shanks transformation applied to $(2/N)|\langle 1|\hat{M}^x_{\rm st}|0\rangle|^2$ twice. The column with three data is the result from the first transformation and the rightmost value is from the second one, which is the best value we can get here. The error is estimated by the difference from the farthest result among the three results of the first transformation. Thus we estimate $(2/N)|\langle 1|\hat{M}^x_{\rm st}|0\rangle|^2 \to 3.86\pm0.06$ $(N\to\infty)$.

N	$(2/N)\lvert\langle 1\rvert\hat{M}^x_{\rm st}\rvert 0\rangle\rvert^2$	Once	Twice
6	2.457 651		
8	2.797 896	3.845 386	
10	3.054 720	3.832 626	3.859 898
12	3.247 799	3.808 645	
14	3.391 431		

$$\lim_{n\to\infty}\frac{P_n-P_\infty}{P_{n-1}-P_\infty}<1 . \tag{36}$$

The result is shown in Table V, where we use the data of $(2/N)|\langle 1|\hat{M}^x_{\rm st}|0\rangle|^2$ for $N=6$, 8, 10, 12, and 14, and apply the transformation twice. We did not use the value for $N=16$ because it leads to misconvergence on the second application of the transformation due to a finite-size effect or a round off. Such a misconvergence sometimes occurs in quantum systems.[4] The result of the second transformation in Table V gives the best estimation we can get, and we determine the error by the difference from the farthest result among the three of the first application of Shanks' transformation. Thus we determine the form of the divergence at H_{c1} as

$$\chi^{xx}_{\rm st}\sim(3.86\pm0.06)\frac{1}{H_{c1}-H} \quad (H<H_{c1}) , \tag{37}$$

at the thermodynamic limit.

Then we give the behavior of $\chi^{xx}_{\rm st}$ for the one-dimensional system at the thermodynamic limit as a solid curve in Fig. 10. The asymptotic forms for $H\sim H_{c1}$ $(H<H_{c1})$ and $H\sim H_{c2}$ $(H>H_{c2})$ are given by (37) and (27), respectively, and always diverges between H_{c1} and H_{c2}.

At last, we return to the quasi-one-dimensional problem. Treating interchain interactions (20) as a mean field, the critical value J_c is given by (21), where we may put $\chi^{\alpha\alpha}_{\rm st}=\chi^{xx}_{\rm st}$. Therefore, within this approximation, we conclude that, however small J is, Néel order exists in the xy plane between H_{c1} and H_{c2}, because $\chi^{xx}_{\rm st}$ of the one-dimensional system diverges for $H_{c1}<H<H_{c2}$. This order is canted Néel order because finite magnetization exists along the z axis here. Thus, if a measurement is done at sufficiently low temperature, canted Néel order can be found for $H_{c1}<H<H_{c2}$. It is consistent with the NMR experiment.[17] In particular, a strong signal could be obtained at $m\simeq\frac{1}{3}$, because the transverse spin correlation is strongest there in the one-dimensional case.

V. CONCLUSION

In this paper the $S=1$ one-dimensional Heisenberg antiferromagnet in a magnetic field at $T=0$ is studied by

numerical diagonalizations up to $N=16$. We gave the magnetization curve at the thermodynamic limit in Fig. 4 and derived that two anomalies exist at H_{c1} and H_{c2} in the curve of dm/dH, but the analytic form of the anomaly at H_{c1} could not be determined. It is also found that the transverse spin correlation decays algebraically and the transverse staggered susceptibility diverges between H_{c1} and H_{c2}. Thus the phase transition at H_{c1} does not break the rotational symmetry in the xy plane yet in one dimension. In quasi-one dimension, however, interchain interactions break it and canted Néel order occurs, within a mean-field approximation for interchain interactions. It is consistent with a recent NMR measurement for NENP at low temperature.

ACKNOWLEDGMENTS

We with to thank Professor Y. Ajiro and Professor S. Maegawa for giving us interesting information about experiments. We also thank Professor Y. Natsume, Professor K. Kubo, Dr. K. Nomura, Dr. J. Suzuki, and Dr. H. Tsunetsugu for fruitful discussions. We used HITAC S-820 in the computer center at University of Tokyo for the numerical calculations.

*Present address: Department of Material Science, Faculty of Science, Himeji Institute of Technology, Kamigori-cho Akogun, Hyogo 678-12, Japan.

[1]F. D. M. Haldane, Phys. Lett. **93A**, 464 (1983); Phys. Rev. Lett. **50**, 1153 (1983).
[2]R. Botet and R. Jullien, Phys. Rev. B **27**, 613 (1983); R. Botet, R. Jullien and M. Kolb, *ibid.* **28**, 3914 (1983); M. Kolb, R. Botet, and R. Jullien, J. Phys. A **16**, L673 (1983).
[3]J. B. Parkinson and J. C. Bonner, Phys. Rev. B **32**, 4703 (1985).
[4]T. Sakai and M. Takahashi, Phys. Rev. B **42**, 1090 (1990).
[5]M. P. Nightingale and H. W. Blöte, Phys. Rev. B **33**, 659 (1986).
[6]I. Affleck, T. Kennedy, E. H. Lieb, and H. Tasaki, Commun. Math. Phys. **115**, 477 (1988).
[7]G. Gómez-Santos, Phys. Rev. Lett. **63**, 790 (1989).
[8]J. P. Renard, M. Verdaguer, L. P. Regnault, W. A. C. Erkelens, J. Rossat-Mignod, and W. G. Stirling, Europhys. Lett. **3**, 945 (1987).
[9]J. P. Renard, M. Verdaguer, L. P. Regnault, W. A. C. Erkelens, J. Rossat-Mignod, J. Ribas, W. G. Stirling, and C. Vettier, J. Appl. Phys. **63**, 3538 (1988).
[10]K. Katsumata, H. Hori, T. Takeuchi, M Date, A. Yamagishi, and J. P. Renard, Phys. Rev. Lett. **63**, 86 (1989).
[11]Y. Ajiro, F. Goto, H. Kikuchi, T. Sakakibara, and T. Inami, Phys. Rev. Lett. **63**, 1424 (1989).
[12]Yu. A. Kosevich and A. V. Chubukov, Zh. Eksp. Theor. Fiz. **91**, 1105 (1986) [Sov. Phys.—JETP **64**, 654 (1987)].
[13]I. Affleck, Phys. Rev. Lett. **62**, 474 (1989).
[14]T. Sakai and M. Takahashi, J. Phys. Soc. Jpn. **58**, 3131 (1989).
[15]H. Tasaki, Phys. Rev. Lett. **64**, 2066 (1990).
[16]T. Sakai and M. Takahashi, Phys. Rev. B **42**, 4537 (1990).
[17]M. Chiba, Y. Ajiro, H. Kikuchi, T. Kubo, and T. Morimoto, in Proceedings of Yamada Conference XXV, J. Magn. Magn. Mater. **90&91**, 223 (1990).
[18]J. L. Cardy, in *Phase Transitions and Critical Phenomena,* edited by C. Domb and J. L. Lebowitz (Academic, London, 1987), Vol. 11, Chap. 2, p. 55.
[19]J. L Cardy, J. Phys. A **17**, L385 (1984); H. W. Blöte, J. L. Cardy, and M. P. Nightingale, Phys. Rev. Lett. **56**, 742 (1986); I. Affleck, *ibid.* **56**, 746 (1986).
[20]J. M. Vanden Broech and L. W. Schwartz, SIAM J. Math. Anal. **10**, 658 (1979).
[21]H. Betsuyaku, Phys. Rev. B **34**, 8125 (1986).
[22]D. Shanks, J. Math. Phys. **34**, 1 (1955).
[23]R. P. Hodgson and J. B. Parkinson, J. Phys. C **18**, 6385 (1985).
[24]T. Sakai and M. Takahashi (unpublished).
[25]M. Takahashi, Phys. Rev. B **38**, 5188 (1988).
[26]A. M. Tsvelik, Phys. Rev. B **42**, 10 499 (1990).
[27]K. Nomura and T. Sakai, Phys. Rev. B (to be published).
[28]I. Affleck, Phys. Rev. B **43**, 3215 (1991).
[29]K. Nomura, Phys. Rev. B **40**, 2421 (1989).
[30]S. Liang, Phys. Rev. Lett. **64**, 1597 (1990).
[31]N. M. Bogoliubov, A. G. Izergin, and V. E. Korepin, Nucl. Phys. **B275** [FS17], 687 (1986).
[32]H. J. Schulz, Phys. Rev. B **34**, 6372 (1986).
[33]M. N. Barber, in *Phase Transitions and Critical Phenomena,* edited by C. Domb and D. L. Lebowitz (Academic, London, 1987), Vol. 8, Chap. 2, p. 145.
[34]D. A. Smith and W. F. Ford, SIAM J. Numer. Anal. **16**, 223 (1979).